Understanding crosstalk in high-resolution color thin-film-transistor liquid crystal displays

by F. R. Libsch
S.-C. A. Lien

Results correlating observed crosstalk-induced color artifacts as a function of the four signal-driving schemes used in high-resolution color thin-film-transistor liquid crystal displays (TFT/LCDs) are presented and theoretically explained. Experimental characterization has been carried out on a high-resolution 146-dot-per-inch, 262K-color, 5.5-in.-diagonal, 480 × 640-pixel (VGA) display. Mathematical modeling and simulations have been developed that help explain the crosstalk-induced color artifacts. The modeling is particularly advantageous for quantifying various tradeoffs between front-of-screen quality and signal-driving schemes when scaling pixel density toward higher-resolution TFT/LCDs.

Introduction

The trend toward larger-diagonal active-matrix liquid crystal display (AMLCD) panel sizes and higher spatial and/or gray-scale resolution has been shown to worsen crosstalk. For example, the trend toward higher-gray-scale-resolution AMLCDs implies controlling the voltage at each pixel location to an equivalent voltage of less than half the least significant bit (LSB) over a frame time. Approximating for the power law of 2.2 (gamma) dependence between front-of-screen luminance observed and gray-scale voltage-level input, a half-level gray-scale resolution for a 6-bit and an 8-bit data driver can be translated respectively into approximately 8- and 3-mV steps. Since crosstalk is only one of several components influencing the pixel voltage value, an incremental increase to another gray-scale bit is meaningful only if crosstalk reduction by at least a factor of 2 is possible [1]. The fundamental root of this worsening crosstalk trend is the relative increase in parasitic coupling capacitance. It has already been shown [2] that, for AMLCDs, a data-line-to-pixel-electrode-separation scaling of 100% from 4 μm to 2 μm, even with a simultaneous data-line-width reduction of 100% from 8 μm to 4 μm, would result in an increase in mutual coupling capacitance of approximately 28%, from 450 to 580 fF/cm. The coupling capacitances between the liquid crystal pixel electrode and the data lines are the source of the data-line-to-pixel (vertical)

0018-8646/98/$5.00 © 1998 IBM

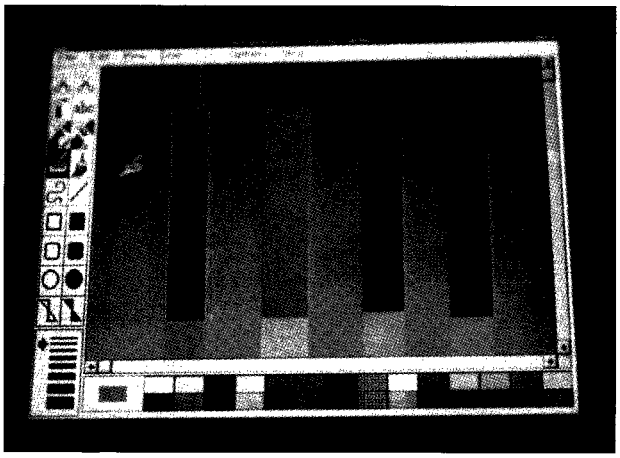

Figure 1

Photograph of front-of-screen image of a 146-dpi, 262K-color, 5.5-in.-diagonal VGA display showing vertical crosstalk artifacts.

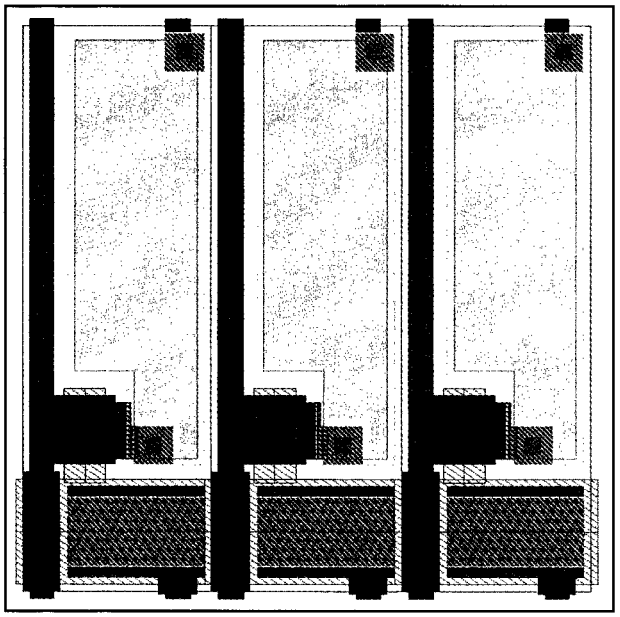

Figure 2

CAD layout of three color subpixels of dimensions 58 μm $\times$ 154 μm, arranged in a vertically striped mode.

crosstalk, whereby information in one row of the display can affect the image on other rows. To abate the inevitable increase of crosstalk with AMLCD scaling still involves some costly sacrifices in reduction of aperture ratio, complicated multilevel data (and gate!) driving schemes at higher power dissipation levels, and added ground-plane fabrication steps incorporating potential yield-lowering defects such as interdielectric pinholes. Particularly absent in the literature is any methodology and/or analysis that extends any of the many crosstalk-related aspects to color displays. Until recently [3, 4], all discussions of crosstalk in the literature had been confined to generic monochrome displays.

This paper focuses on quantifying and understanding a front-of-screen color-dependent image pattern artifact, with origins found to be in vertical crosstalk. To this end, a mathematical treatment is provided for evaluating driving schemes used commercially to compensate for crosstalk with respect to their effect on color-dependent image artifacts. To show the effect on crosstalk of the current AMLCD scaling trend, a 146-dot-per-inch (dpi), 162K-color (6 gray-scale bits per color), 5.5-in.-diagonal, 480 $\times$ 640 (VGA) display has been fabricated to mimic one fourth of an intended display design point of a future 11.2-in.-diagonal color Super-XGA (1280 $\times$ 1024-pixel) display.

Color-dependent image pattern artifacts

Figure 1 shows a photograph of a color bar-code image displayed on a 146-dpi, 262K-color, 5.5-in.-diagonal, 480 $\times$ 640 (VGA) display. The image, created by the software "Paintbrush," has been intentionally drawn to have four color bar codes of red, green, blue, and black, from left to right, respectively. The background of the image has been selected to be 50% gray, or 50% maximum transmission through each of the three different subpixels of red, green, blue (RGB). What have not been drawn intentionally, but are present owing to vertical crosstalk, are the regions above and below the four color bars. Above each color bar is the same color in a darker hue, and below each color bar, the complementary color. For example, below the red, green, blue, and black bars are the complementary colors of cyan, magenta, yellow, and white, respectively. Closer inspection through an eye loop of the magenta region, for example, shows green subpixels slightly brighter than, and red subpixels slightly darker than, the 50% gray background immediately to the left or to the right of the red color bar code. The blue pixels' change in brightness, if any, remains undetectable to the eye. Although the literature does not deal with color crosstalk artifacts, what is mentioned [4] is the standard monochrome black rectangle, surrounded by a lighter and darker luminance of gray below and above the black rectangle, respectively. The published effects are in agreement with those observed around the black bar when vertical crosstalk is present. However, we show that some opposite-image artifacts (for example, a monochrome black rectangle, now surrounded by a darker and lighter luminance of gray below and above a black rectangle pattern, respectively) can also be possible and are mathematically explainable.

Figure 2 shows the CAD layout of three subpixels from the 146-dpi display of Figure 1. Six masking steps are used to form the staggered inverted trilayer TFT structure; the steps are chronologically labeled as (mask 1—pink) for patterning of indium–tin-oxide (ITO) pixel electrodes; (mask 2—45° diagonal blue hatched) for patterning of Cu TFT gates and gate lines; (mask 3—red) for patterning of plasma-enhanced chemical vapor deposition (PECVD) of SiN_x/a-Si:H/SiN_x TFTs, storage capacitors, crossover trilayer, and wet etching of an upper SiN_x layer; (mask 4—brown crosshatched) for patterning of PECVD heavily phosphor-doped microcrystalline TFT source and drain contacts; (mask 5—dark blue) for patterning of Mo/Al/Mo data lines and contacts; and (mask 6—not shown for clarity) for patterning of PECVD SiN_x passivation layer [5]. The key design parameters of the 146-dpi display are summarized in **Table 1**. The capacitances, which determine the immunity to vertical crosstalk, are described in the next section.

Table 1 Key design parameters for 146-dpi display.

Parameter	*Value*
Display diagonal	5.5
Spatial resolution	480 × 640 × 3
Density	146 dpi
Subpixel	58 μm × 154 μm
Frame refresh rate	75 Hz
Data-driving method	Frame inversion
Aperture ratio	45%
Colors	262,144
Process steps	6
TFT width-to-length	7 μm/8 μm
TFT gate-to-source overlap capacitance	21.25 fF
Liquid crystal cell-gap thickness, H	5 μm
Gate-line width, material	25 μm, Cu
Data-line width, material, W	8 μm
Data line-to-pixel-electrode separation	4 μm
Data-line-to-pixel capacitance, C_{PD}	4.73 fF
Adjacent-data-line-to-pixel capacitance, $C_{PD'}$	5.99 fF
Pixel-to-gate-line capacitance, C_{PG}	1.63 fF
Pixel-to-adjacent-gate-line capacitance, $C_{PG'}$	1.90 fF
Storage capacitance, C_S	70.0 fF
Minimum liquid crystal capacitance, C_{LCmin}	45.0 fF
Maximum liquid crystal capacitance, C_{LCmax}	90.0 fF
Gate-line time constant	917 ns
Scan time	27.8 μs

Data-line-to-pixel capacitive coupling

Display crosstalk is the undesired artifact resulting when the intended root-mean-square (RMS) gray-scale voltage across the liquid crystal (LC) is altered by the following mechanisms: 1) incomplete pixel charging current due to such factors as unequal data-driver loading, low thin-film-transistor (TFT) transconductance, and line waveform distortion and delay; 2) leakage current from the pixel through the TFT or LC; and 3) displacement currents caused by parasitic capacitive coupling of the pixel to both adjacent signal-line voltage changes. Note that mechanism 1 occurs during the scan time of the pixel transistors' on state, while mechanisms 2 and 3 occur during their off state. The interdependent remedies to the three mechanisms above are based on material selection and fabrication process conditions, device design and layout, and driving schemes. For the 146-dpi display, the use of a low-crossover capacitance design and the selection of higher-conductivity metals such as Cu scan lines [5] and Mo/Al/Mo data lines eliminate incomplete pixel charging from line waveform distortion and delay, even at a refresh rate of 75 Hz. The copper gate scan lines' low resistivity of 2 μΩ-cm allows a gate charging time of approximately 16 μs and a gate-line delay sufficiently small to charge the pixel to within 100 mV of the data signal voltage for an SXGA (11.2 in., 146 dpi) display. Similarly, incomplete pixel charging from low-transconductance a-Si:H TFTs has been eliminated through process-related mobility improvements and the use of a minimum channel length of 7 μm. To minimize mechanism 2, the 146-dpi display is fabricated with an integrated black matrix to perform as a light shield for minimizing photogenerated leakage currents in the a-Si:H TFTs [4, 6]. The influence of photogenerated TFT currents is currently under investigation, but low enough levels of leakage and photogenerated currents with a backlight luminance approaching 10^{-13}–10^{-14} A/μm are desired. The LC material incorporated has bulk resistivities in the range of 10^{12} Ω-cm.

Finally, the displacement currents caused by parasitic capacitive coupling are an increasingly troublesome by-product of scaling to smaller lithographic dimensions and tighter ground rules. The ratio of parasitic capacitive coupling between the pixel-to-data line (α) and pixel-to-adjacent-data line (β) are shown in the layout of **Figure 3**. From the crosstalk capacitance equivalent circuit of **Figure 4**, α and β can be expressed as

$$\alpha = \frac{C_{PD}}{C_{LC} + C_S + C_{PG} + C_{PG'} + C_{GS} + C_{PD} + C_{PD'}}, \quad (1)$$

$$\beta = \frac{C_{PD'}}{C_{LC} + C_S + C_{PG} + C_{PG'} + C_{GS} + C_{PD} + C_{PD'}}, \quad (2)$$

where C_{PD} and $C_{PD'}$ are the data-line- and adjacent-data-line-to-pixel-electrode coupling capacitances, respectively; C_{PG} and $C_{PG'}$ are the gate-line- and adjacent-gate-line-to-pixel-electrode coupling capacitances, respectively; C_{LC} is the liquid crystal capacitance between the common electrode and the pixel electrode; C_S is the storage capacitance between the adjacent gate line and the pixel electrode; and C_{GS} is the TFT gate-to-source parasitic

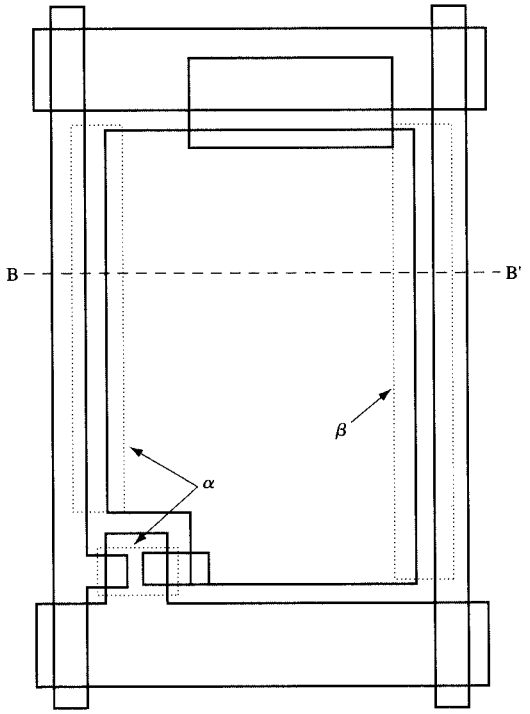

Figure 3

Top view of a typical pixel layout for a TFT/LC array, showing the data-line-to-LC-electrode parasitic capacitance regions. See Figure 6 for a cross-sectional view along the line BB'.

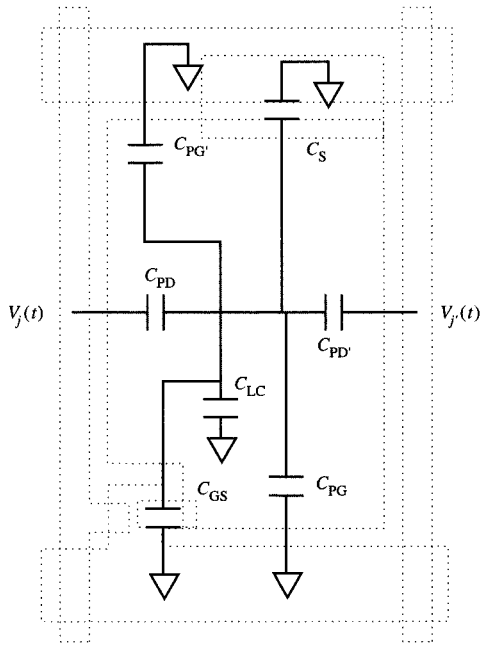

Figure 4

Equivalent circuit for capacitive coupled transmission-line analysis of pixel layout designs for crosstalk evaluation. For simplicity, the mutual capacitance of the top-plate common electrode is not shown.

overlap capacitance. For the 146-dpi display, calculated capacitances from the pixel layout (listed in Table 1) are C_{PG} = 1.63 fF, $C_{PG'}$ = 1.90 fF, $C_{LC_{min}}$ = 45 fF, C_S = 70 fF, and C_{GS} = 21.25 fF. Note also that the data-line-to-pixel-electrode coupling capacitances, C_{PD} and $C_{PD'}$, are not fixed and are a function of the twisted nematic liquid crystal state. The twisted nematic liquid crystal dielectric constant is lowest, and, hence, the liquid crystal capacitance is minimal when in the white mode (lowest voltage across C_{LC}) for the normally white mode 146-dpi display, and in that state the corresponding data-line- and adjacent-data-line-to-pixel-electrode couplings, i.e., α and β, are usually increased. Note that all capacitances except C_S in Equations (1) and (2) are a function of the twisted nematic liquid crystal dielectric constant, and specific values are needed to calculate whether α and β will increase or decrease.

Figure 5 shows the worst-case ($C_{LC_{min}}$) calculated C_{PD} and $C_{PD'}$ design values illustrating the tradeoffs in data-line width/liquid-crystal-cell-gap thickness, W/H, and pixel-electrode spacing/liquid-crystal cell gap, S/H. Obtained for the 146-dpi display is the data-line- and adjacent data-line-to-pixel-electrode W/H ratio of 8 μm/5 μm = 1.6, an S/H ratio of 4 μm/5 μm = 0.8, and a resulting mutual coupling capacitance of 0.45 pF/cm. The TFT source-to-drain electrode values are a W/H ratio of 16 μm/5 μm = 3.2, an S/H ratio of 2 μm/5 μm = 0.4, and a resulting mutual coupling capacitance of 0.72 pf/cm. To first order, $C_{PD'}$ = 6.08 fF, and is calculated from the ITO pixel electrode length of 132 μm; C_{PD} = 5.98 fF, and is calculated from the pixel electrode length of 104 μm and the TFT source-to-drain electrode length of 18 μm. Future scaling trends toward smaller lithographic dimensions and tighter ground rules will diminish the data-line width (W) and the pixel-to-data-line spacing (S). For example, with a data-line-to-pixel separation S, scaling of 100% from 4 μm to 2 μm increases the mutual capacitance by approximately 38% from 450 to 620 fF/cm, while a reduction of 100% in W from 8 μm to 4 μm decreases the mutual coupling capacitance by approximately 11%, from 450 to 400 fF/cm. The result is a net increase in mutual coupling capacitance by approximately 27%, from 450 to 575 fF/cm. The scaling trend is therefore a gradient toward the left/upper-left of Figure 5, providing an increase in the mutual coupling capacitance. For the calculations it was assumed that the

display cross section shown in **Figure 6** is applicable; a conducting ITO plane (common electrode) is assumed to exist a dimension H above the data line and the pixel electrode, and the data line and pixel electrode are treated as coupled microstrip lines separated by dimension S. The anisotropic property of the liquid crystal produces a voltage-dependent dielectric constant. For the 146-dpi display, the corresponding bulk dielectric values range between $4\varepsilon_0$ and $8\varepsilon_0$, where ε_0 is the permittivity of vacuum. The values indicated in Figure 5 assume a coupled microstrip structure [7] with a film thickness of 100 nm for the data metal and the pixel electrode and a dielectric constant of $4\varepsilon_0$ for the liquid crystal and the insulating glass substrate. The coupling capacitance is reduced as the dielectric constant for the liquid crystal increases relative to the dielectric constant of the glass. In addition, the coupling between two adjacent lines with no nearest neighbors is greater than the equivalent coupling that would occur in a periodic array, since field sharing would be expanded to include other conductors in the system. Thus, the analysis of only the two-line coupled structure with surrounding dielectrics of equal dielectric constants should yield a good baseline (worst case) for crosstalk-cancellation design purposes.

The calculated parasitic data-line-to-pixel coupling ratio values from Equations (1) and (2) as a function of the pixel capacitances from Table 1 and with $C_{PD} = 5.98$ fF and $C_{PD'} = 6.08$ fF yield $\alpha \approx \beta \approx 0.040$. Clearly, decreasing α and β must be accomplished if successful crosstalk elimination is to take place. One method for minimizing α and β would be to increase C_S. Another method would be to provide ground-plane shielding beneath the data line. Both of these methods would require added pixel area, at the expense of a smaller aperture ratio and larger gate-line delay. Besides, at that stage the 146-dpi display has already been fabricated, and a cell redesign and/or process alteration would prove time-consuming and costly. The third approach, that of providing an appropriate data-driving scheme, would leave unaltered the pixel layout and fabrication technology, and might provide the least expensive and most straightforward approach to further pixel scaling. Note that this approach does not change α and β, but relies on incorporating some form of positive and negative data-line pulse-coupling cancellation. On the down side, higher voltage drivers and/or higher driver power consumption may result. Selection of the proper driving method is investigated in the next section.

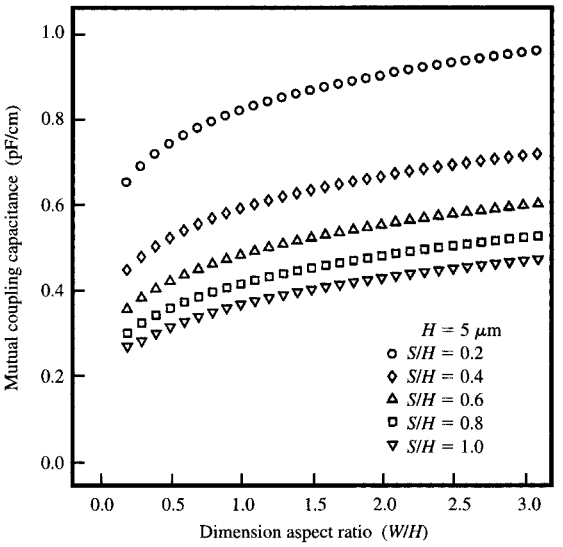

Figure 5

Mutual coupling capacitance. Calculations are based on an asymmetrical microstrip line model for which the following are assumed: data metal and pixel electrode, both having a width W, a thickness of 100 nm, a separation S, and a common-electrode ground plane located a distance H above, as characterized by Figure 4.

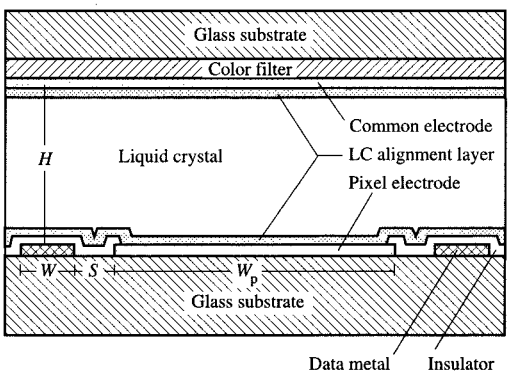

Figure 6

Schematic cross-sectional view along the line BB' of Figure 3. H is the top-plate gate-electrode-to-data-line distance, W is the data-line width, S is the data-line-to-LC-pixel-electrode spacing, W_p is the pixel electrode width, and $W + 2S + W_p$ is the pixel pitch.

Analysis of crosstalk elimination using driving methods

The value of the instantaneous voltage V_{pi} across the liquid crystal capacitor in the ith row position for the standard configuration is given by

$$V_{pi}(t) = V_i + \alpha[V_j(t) - V_i] + \beta[V_{j'}(t) - V_{i'}]. \quad (3)$$

V_i and $V_{i'}$ are the data voltages initially written onto the pixel and adjacent pixel through pixel selection, respectively, through their corresponding TFTs. $V_j(t)$ and $V_{j'}(t)$ are the data-line and adjacent-data-line voltages with parasitic coupling factor to the pixel, α and β, respectively (see Figure 4). When a dc voltage is placed across the liquid crystal (LC), the ions present in it drift to the electrodes, creating an internal electric field that counteracts the dc externally applied field. These ions at the electrodes will resist any voltage stimulus of the same polarity, so that no or little LC luminance transmission change is possible. To avoid this situation, all present driving methods allow for some signal voltage polarity inversion in a time scale shorter than that needed for the mobile LC ions to move substantially. The LC thus responds to the root mean square (RMS) of the signal inversions. Signal-inversion periods are either frame-time-in-data-line (DI) and frame (FI) driving methods, or line-time-in-gate-line (GI) and dot (D) driving methods. The data-line signal polarities coupling into pixels are reversed between every data line, gate line, or both data and gate lines in the DI, GI, and D methods, respectively. There are tradeoffs among the four mentioned driving methods [1], with the main ones being the degree of crosstalk cancellation vs. data-driver chip power dissipation. In general, in today's displays, TAB (tape automated bond) or COG (chip on glass) data drivers are mounted only along one side to decrease the non-active display area and thus minimize the module package size. The one-side-attached data-driver display implies that only the FI and GI driving methods can use low-voltage data drivers, provided that the GI driving method simultaneously modulates the common electrode. In addition, frame time-inversion driving methods of FI and DI provide a low row-charging current. The 146-dpi display with front-of-screen output shown in Figure 1 utilizes the DI driving method at a 75-Hz frame rate. For reasons of low row-charging currents with modest crosstalk cancellation, we first analyze the DI driving method used in the 146-dpi display, and then compare crosstalk results for the FI, GI, and D driving methods.

For the DI driving method, where each consecutive signal line has alternating positive and negative data polarity and the data polarity is inverted once per frame time, the RMS voltage at the ith row position at the LC can be derived from Equation (3) as

$$[V_{\mathrm{pi}}(RMS)]^2 = \frac{1}{N}\left\{ V_i^2 + \sum_{j>i}^{N} [V_i - \alpha(V_i - V_j) - \beta(V_{i'} - V_{j'})]^2 + \sum_{j=1}^{i-1} [V_i - \alpha(V_i + V_j) - \beta(V_{i'} + V_{j'})]^2 \right\}. \quad (4)$$

In applying the DI driving method to analyze the locations TR, TG, TB, TBK, and BR, BG, BB, BBK (vertically above and below the color and black bar codes) in Figure 1 for the vertically arranged RGB subpixel pattern, note that the subpixel data-line voltage and adjacent data-line voltage for display regions inside the colored bars are not equal for two of the possible three pairs of adjacent data lines that straddle each subpixel. In other words, for two pairs of adjacent data lines (two subpixels), $V_i(t) \neq V_{i'}(t)$ and $V_j(t) \neq V_{j'}(t)$; for the third pair of adjacent data lines (one subpixel), $V_i(t) = V_{i'}(t)$ and $V_j(t) = V_{j'}(t)$ in the region of the intentionally written red, green, blue, and black color bars. Note that the black bars differ in that for all three pairs of adjacent data lines, $V_i(t) = V_{i'}(t)$ and $V_j(t) = V_{j'}(t)$. In the green bar area, the RGB subpixels are each straddled by two data lines contacting the R and G, G and B, and B and R subpixels, respectively. Since the green bar is composed of 100% transmission through the G subpixels and 0% transmission through the B and R subpixels, only the B subpixel is straddled by the same voltage from the B data line (V_j) and the R data line ($V_{j'}$), where $V_j = V_{j'}$. This corresponds to the observance, at area BG, where the green pixels are darker and the red pixels lighter than the 50% gray reference area; there is no observed difference in the blue pixels. By neglecting the second-order crosstalk term in Equation (4), we can obtain a simplified expression

$$[V_{\mathrm{pi}}(RMS)]^2 \cong (V_i - \alpha V_i + \beta V_{i'})^2 + \frac{2}{N}\alpha V_i\left[\sum_{j\geq i}^{N} V_j - \sum_{j=1}^{i-1} V_j\right] - \frac{2}{N}\beta V_i\left[\sum_{j\geq i}^{N} V_{j'} - \sum_{j=1}^{i-1} V_{j'}\right]. \quad (5)$$

Notice that the data $V_j(t) \neq V_{j'}(t)$ guarantee that the first-order term (linear in α and β) in Equation (5) is dependent on the data-line voltage for one frame, and make the RMS pixel voltage pattern-dependent or screen-image-pattern-dependent. The DI driving scheme contains an additional first-order crosstalk term; for example, in area BG the G pixels are dimmer and the R pixels have higher luminance than the intended 50% luminance because of the substantial increase in crosstalk. For the blue-pixel data-line voltage and the adjacent data line belonging to the red pixel, $V_i(t) = V_{i'}(t)$ and $V_j(t) = V_{j'}(t)$, so that there are no first-order effects on the blue pixel other than the gradual background vertical shading characteristic of all frame time-inversion methods (DI, FI) that rely only on data value polarity permutations. (Other frame time-inversion methods[1] [2, 8] that introduce a compensation pulse level between the data values achieve

[1] S. A. Lien and F. R. Libsch, U.S. patent pending.

a uniform background, eliminating vertical background vertical shading.) The resulting color is then magenta beneath the green bar, or, in general, the complement of that of the color bars.

Notice that the gradual background vertical shading of the blue pixel is predicted by Equation (5) from the nonzeroing of the first-order terms when the difference of sums of the second and third terms on the right-hand side as the data-line voltages following the ith row position to the end of the frame ($j > i$ to N) is unequal to the sum of the data-line voltages from the beginning of the frame to the ith row position ($i = 1$ to $i - 1$). Because the resistivity of the 146-dpi display LC is high enough (10^{12} Ω-cm) and the storage capacitance amply large to produce more than a 95% holding ratio, the effects of the decay of the liquid crystal voltage have been neglected for simplicity. They are easily added [1] and do not change the conclusion. The charge-holding characteristics and display performance as a function of backlight intensity have been studied and have been reported in [6]. The transistor charge-holding characteristics and the display have good performance and good image quality at a backlight intensity of 3000 cd/m^2.

Similarly, a general expression can be written for the case of the FI driving method, for which each signal line has the same data polarity and the data polarity is inverted once per frame time. We thus obtain

$$[V_{pi}(RMS)]^2 = \frac{1}{N}\left\{V_i^2 + \sum_{j>i}^{N}[V_i - \alpha(V_i - V_j) - \beta(V_{i'} - V_{j'})]^2 + \sum_{j=1}^{i-1}[V_i - \alpha(V_i + V_j) - \beta(V_{i'} + V_{j'})]^2\right\}. \quad (6)$$

By neglecting the second-order crosstalk terms (α^2, β^2, and $\alpha\beta$) in Equation (6), we obtain a simplified expression,

$$[V_{pi}(RMS)]^2 \cong (V_i - \alpha V_i + \beta V_{i'})^2 + \frac{2}{N}\alpha V_i\left[\sum_{j\geq i}^{N} V_j - \sum_{j=i}^{i-1} V_j\right] + \frac{2}{N}\beta V_i\left[\sum_{j\geq i}^{N} V_{j'} - \sum_{j=i}^{i-1} V_{j'}\right]. \quad (7)$$

Similarly, for the case of the GL driving method, where each signal line has the same data polarity and the data polarity is inverted once per scan line time, we obtain

$$[V_{pi}(RMS)]^2 = \frac{1}{N}\left\{V_i^2 + \sum_{j(\text{even})>i}^{N}[V_i - \alpha(V_i + V_j) - \beta(V_{i'} + V_{j'})]^2 + \sum_{j(\text{even})>1}^{i-1}[V_i - \alpha(V_i - V_j) - \beta(V_{i'} - V_{j'})]^2 + \sum_{j(\text{odd})>i}^{N}[V_i - \alpha(V_i - V_j) - \beta(V_{i'} - V_{j'})]^2 + \sum_{j(\text{odd})=1}^{i-1}[V_i - \alpha(V_i + V_j) - \beta(V_{i'} + V_{j'})]^2\right\}. \quad (8)$$

By neglecting the second-order crosstalk terms (α^2, β^2, and $\alpha\beta$) in Equation (8), we obtain the simplified expression

$$[V_i(RMS)]^2 \approx (V_i - \alpha V_i + \beta V_{i'})^2 + \frac{2}{N}\alpha V_i\left[\sum_{j(\text{even})>1}^{i} V_j - \sum_{j(\text{even})>i}^{N} V_j - \sum_{j(\text{odd})=1}^{i-1} V_j + \sum_{j(\text{odd})\geq i}^{N} V_j\right] + \frac{2}{N}\beta V_i\left[\sum_{j(\text{even})>1}^{i} V_{j'} - \sum_{j(\text{even})>i}^{N} V_{j'} - \sum_{j(\text{odd})=1}^{i-1} V_{j'} + \sum_{j(\text{odd})\geq i}^{N} V_{j'}\right]. \quad (9)$$

Compared to the FI driving method described by Equation (7), the GI driving scheme contains an additional polarity reversal, as is evident from the separation of even and odd data-line values (V_j) and adjacent data-line ($V_{j'}$) values. For this reason, the GI driving method, in general, provides better crosstalk compensation than the FI driving method, but this is not guaranteed, because the magnitude of crosstalk is dependent upon the screen image pattern. For example, if an alternating image pattern of black to white on the spatial periodicity of a scan line were present, the even scan-line data values (V_j for j being even) would negate the minus sign and add to the odd scan-line data values (V_j for j being odd) in the second term, and the even scan-line adjacent data values ($V_{j'}$ for j' being even) would negate the minus sign and add to the odd scan-line time adjacent data values ($V_{j'}$ for j' being odd) in the third term, resulting in the worst-case adding of all coefficients of α and β for the case of the GI driving method. In general, image patterns tend to be uniform over a screen area of at least several gate-line spatial dimensions.

The FI and GI methods may produce zero net data-line voltage summations for a given pixel in a few given image screen patterns, and thus may lead to a zero first-order crosstalk term. In addition, the GI method may produce zero net data-line voltage summation for all pixels in some given image patterns.

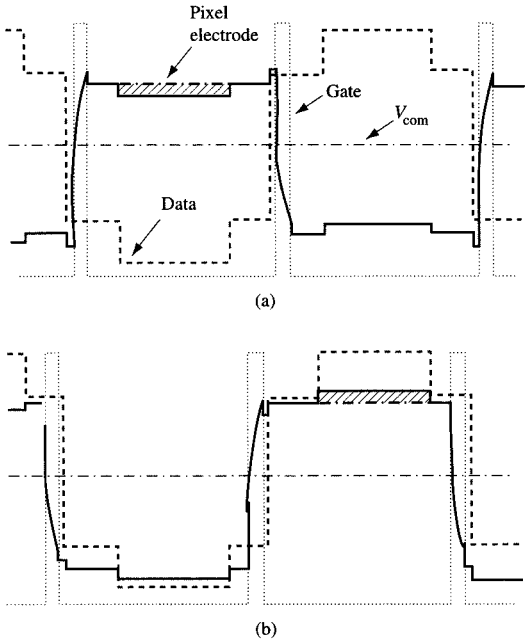

Figure 7

DI driving method pixel waveform voltages, with $\alpha < \beta$ for two regions corresponding to the color-bar data-line pixels (a) above and (b) below the color-bar pattern of Figure 1. The same pixel waveform voltage is representative of the regions (a) above and (b) below the black-bar pattern. V_{com} is the common-mode voltage applied to the counter electrode of the liquid crystal.

As above, a general expression can be written for the case of the dot inversion driving method (D), where the DI and the GI driving methods are both applied to the data so that each consecutive signal line (DI) as well as each consecutive gate line (GI) has an alternating positive and negative data polarity, and the data polarity is inverted once per frame time. The resulting expression is

$$[V_{pi}(RMS)]^2 = \frac{1}{N}\left\{V_i^2 + \sum_{j(\text{even})>i}^{N} [V_i - \alpha(V_i + V_j) + \beta(V_{i'} + V_{j'})]^2 + \sum_{j(\text{even})=1}^{i-1} [V_i - \alpha(V_i - V_j) + \beta(V_{i'} - V_{j'})]^2 + \sum_{j(\text{odd})>i}^{N} [V_i - \alpha(V_i - V_j) + \beta(V_{i'} - V_{j'})]^2 + \sum_{j(\text{odd})=1}^{i-1} [V_i - \alpha(V_i + V_j) + \beta(V_{i'} + V_{j'})]^2\right\}. \quad (10)$$

By neglecting the second-order crosstalk terms (α^2, β^2, and $\alpha\beta$) in Equation (10), we obtain the simplified expression

$$[V_i(RMS)]^2 = (V_i - \alpha V_i + \beta V_{i'})^2 + \frac{2}{N}\alpha V_i\left[\sum_{j(\text{even})>1}^{i} V_j - \sum_{j(\text{even})>i}^{N} V_j - \sum_{j(\text{odd})=1}^{i-1} V_j + \sum_{j(\text{odd})\geq i}^{N} V_j\right] - \frac{2}{N}\beta V_i\left[\sum_{j(\text{even})>1}^{i} V_{j'} - \sum_{j(\text{even})>i}^{N} V_{j'} - \sum_{j(\text{odd})=1}^{i-1} V_{j'} + \sum_{j(\text{odd})\geq i}^{N} V_{j'}\right]. \quad (11)$$

Comparing Equations (5), (7), (9), and (11) for all four crosstalk-reduction driving methods shows a gain-correction term $(V_i - \alpha V_i + \beta V_{i'})^2$ as the first term on the right-hand side. For a simplified case, if $V_i = V_{i'}$, the gain correction is $(1 - \alpha \pm \beta)^2$, and the effect is only a parallel shift in the transmission vs. voltage (T-V) curve which depends on the values of α and β. Any dc gain in the required RMS operation of the LC can easily be offset. However, in general, $V_i \neq V_{i'}$, which makes the gain term data dependent on the voltage or image pattern, and it cannot be easily offset. For completeness, we mention that all of the above conventional driving methods (DI, FI, GI, D) in general exhibit first-order crosstalk, as indicated by Equations (5), (7), (9), and (11). A recent data complement (DC) method [8, 9] applied to the frame time inversion of data (FI or DI) eliminates first-order crosstalk by providing the data complement for each data value when the gate line is inactive. It is clear that the DC method requires that a fraction of the line time (typically one half) be devoted to the compensation signals, with the TFTs turned off. As a result, use of that method demands a factor-of-2 increase in switching speed. Another method, the precharge compensation method (CC)[1] [7], eliminates first-order crosstalk and, in the worst case, achieves at least the same crosstalk elimination as the DC method, but, in addition, uses the entire scanning time to charge the pixels. Because of the elimination of the first-order crosstalk term, the CC driving method is not dependent upon the front-of-screen image pattern, as are the driving methods discussed above.

Simulation results

The color aspect of the image pattern dependency is explained below by calculations based on the DI driving method described by Equation (4) applied to the color bar pattern shown in Figure 1. The simulations have been performed for a color-bar and black-bar pattern for which the bar-pattern voltage was present continuously from gate lines 126 through 384, inclusive. For example, in the green-bar pattern area, the green data-line voltage was set to

100% transmission, or V_j = 1.0 V, for j = 126–384, while the red and blue data-line voltages were set to 0% transmission, or $V_{j'}$ = 4.50 V, for j' = 126–384, while the gate lines less than 126 and greater than 384 for all remaining RGB data lines were fixed to 50% light transmission, or $V_j = V_{j'}$ = 2.15 V, for j, j' = 1–125 and j, j' = 385–480. For the 146-dpi display, a normally white-mode twisted nematic liquid crystal is used with the white (100% transmission), black (0% transmission), and gray (50% transmission) levels given by 1, 2.15, and 4.5 V, respectively. To gain insight, the simulations below treat two cases, $\alpha < \beta$ and $\alpha > \beta$.

Figure 7 shows the voltage waveforms for the DI driving method, illustrating the data line, scan line, and pixel-electrode waveform for the 100% transmitting color-bar pixel when $\alpha < \beta$. Since β dominates, the adjacent data-line waveform is shown. The crosshatched area on the pixel waveform represents the difference from what is calculated on a horizontally adjacent pixel that is 50% on without the color-bar influence, or written to 2.15 V, to what is actually calculated from the adjacent data-line coupling (β) and from the data line producing the color bar. Note that the crosshatched area represents the voltage vs. time difference between a 50% transmitting neighboring pixel without crosstalk (higher voltage and darker state), and a pixel in the area above the color bar with crosstalk (lower voltage and brighter state), both addressed by the same gate line. Figure 7(b) represents the pixel waveform voltage corresponding to a pixel in the area below the color bar exhibiting crosstalk, resulting in a higher gray-scale voltage, or darker state. So, for example, for the green bar, the green pixels above the green bar are in a lighter state, and below the green bar, in a darker state than a 50% transmitting horizontally nearby pixel area. In **Figures 8** and **9**, simulations with α = 0.03 and β = 0.04 are plotted along with the measured LC normalized transmission vs. voltage curve that corresponds to the pixel waveform for the area above [Figure 7(a)] and below [Figure 7(b)] the color bar, respectively. Above and below the color bar, the voltages of color-line pixels (for example, the green pixels for the green color bar), are respectively lower (brighter) or higher (darker) by approximately 70 mV. Since 100 mV produces a transmission change of approximately 10% around the 50% transmission point, this translates into 7% more or less transmission. Above and below the color bar, the voltages of adjacent pixels to the left (for example, the red pixels for the green color bar) are correspondingly higher (darker) and lower (brighter) by approximately 64 mV, respectively. This translates into approximately 6.4% less or more light transmission for adjacent color-bar data-line pixels above gate line 126 and below gate line 384, respectively. The remaining adjacent pixels to the right (for example, the blue pixels for the green color bar)

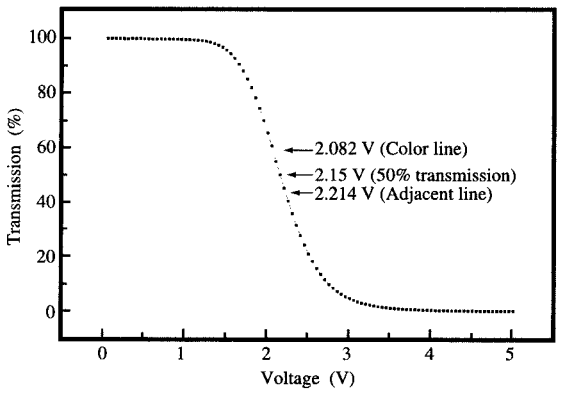

Figure 8

Transmission vs. voltage data with crosstalk simulation voltages, with α = 0.03 and β = 0.04, for the region corresponding to the color-bar data-line pixels above the color-bar pattern of Figure 1.

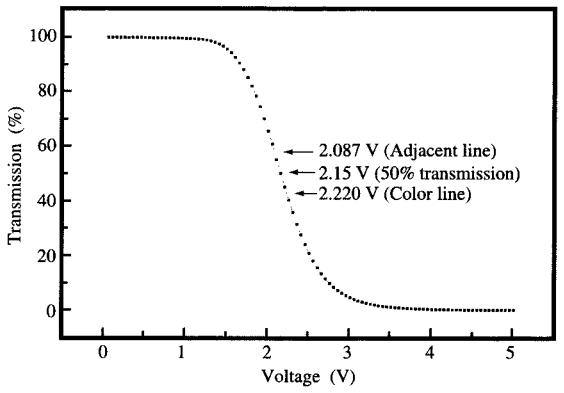

Figure 9

Transmission vs. voltage data with crosstalk simulation voltages, with α = 0.03 and β = 0.04, for the region corresponding to the color-bar data-line pixels below the color-bar pattern of Figure 1.

have no crosstalk-induced voltage or corresponding transmission change from 2.15 V or 50% transmission, respectively. These color artifacts are in agreement with what is observed in Figure 1.

The area of the display in Figure 1 above or below the black bar can be represented by the same voltage waveform shown in Figure 7. Notice that, unlike the pixels in the color-bar region, all three RGB pixels are at the same voltage, and therefore display the same corresponding

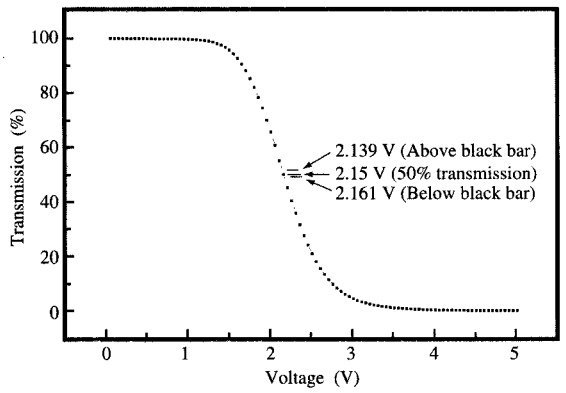

Figure 10

Transmission vs. voltage data with crosstalk simulation voltages, with $\alpha = 0.03$ and $\beta = 0.04$, for the region corresponding to the black-bar data-line pixels above and below the black-bar pattern of Figure 1.

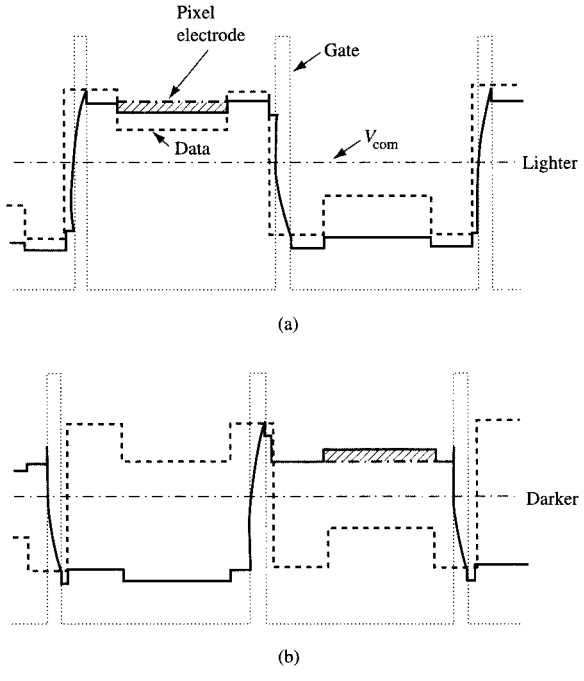

Figure 11

DI driving method pixel waveform voltages, with $\alpha > \beta$, for two regions corresponding to the color-bar data-line pixels (a) above and (b) below the color-bar pattern of Figure 1.

crosstalk in the black-bar area ($V_j = V_{j'} = 4.5$ V for $j, j' = 126$–384), as well as above and below the black-bar area ($V_j = V_{j'} = 4.5$ V for $j, j' < 126$ or $j, j' > 384$). Simulations with $\alpha = 0.03$ and $\beta = 0.04$ plotted along with the measured LC normalized transmission vs. voltage curve in **Figure 10** show an increase or decrease of 11 mV, or 1.1% transmission, for the pixels in the region above and below the black bar, respectively. However, Figure 1 shows the opposite, namely a darker than 50% gray-scale transmission level above the black bar, and a brighter than 50% gray-scale transmission level below the black bar.

To fully understand this artifact, we now analyze the case of $\alpha > \beta$, the simulation case for which $\alpha = 0.08$ and $\beta = 0.03$. **Figure 11(a)** shows the color-bar data-line pixel waveform in the region above a color bar, resulting in a lower gray-scale voltage, or a lighter state for a fraction of the frame time by the amount indicated by the crosshatched area, compared to that of a 50%-transmitting pixel. **Figure 11(b)** shows the pixel waveform voltage corresponding to the area below the color bar, resulting in a higher gray-scale voltage, or darker state. The net polarity direction of the pixel electrode coupling is identical to the previously analyzed case of $\alpha < \beta$. Above (**Figure 12**) and below (**Figure 13**) the color bar, the voltages of the color-bar data-line pixels are lower (brighter) or higher (darker) by approximately 87 mV (8.7% transmission change), respectively. Above and below the color bar, the voltages of the adjacent pixels to the left are correspondingly higher (darker) and lower (brighter) by approximately 120 mV (12% transmission change), respectively. There are no crosstalk-induced voltages or corresponding transmission changes from 2.15 V or 50% transmission levels, respectively, on the remaining adjacent pixels to the right. Therefore, the color-bar complementary color below the color bar and the brighter color bar color above the color bar are realized by both cases of $\alpha > \beta$ and $\alpha < \beta$.

The areas of the display of Figure 1 above and below the black bar can be represented by the voltage waveform shown in **Figure 14**. Notice that, in contrast to the pixels above and below the color bar, all three RGB pixels have the same voltage, and therefore they display the same corresponding crosstalk in the black-bar area ($V_j = V_{j'} = 4.5$ V for $j, j' = 126$–384), as well as above and below that area ($V_j = V_{j'} = 4.5$ V for $j, j' < 96$ or $j, j' > 384$). Simulations with $\alpha = 0.08$ and $\beta = 0.03$ plotted along with the measured LC normalized transmission vs. voltage curve in **Figure 15** show an increase or decrease of approximately 65 mV, or 6.5% transmission, for the pixels in the area above or below the black bar, respectively. A difference of approximately 7% in level of luminance is experimentally observed for the display of Figure 1 between pixels addressed by the same gate line for the

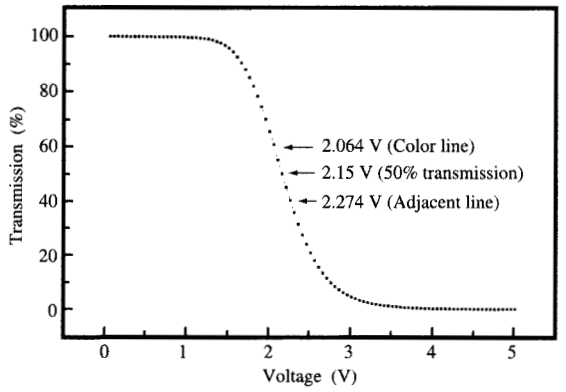

Figure 12

Transmission vs. voltage data with crosstalk simulation voltages, with $\alpha = 0.08$ and $\beta = 0.03$, for the region corresponding to the color-bar data-line pixels above the color-bar pattern of Figure 1.

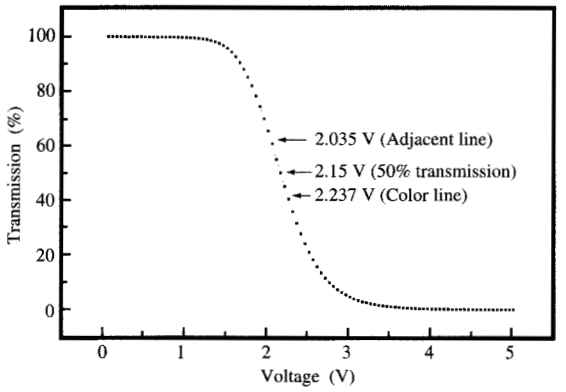

Figure 13

Transmission vs. voltage data with crosstalk simulation voltages, with $\alpha = 0.08$ and $\beta = 0.03$, for the region corresponding to the color-bar data-line pixels below the color-bar pattern of Figure 1.

50% transmission region (no bar patterns) and the regions below and above the black bar. Notice that the appearance of the display of Figure 1 is in accord with the simulations, that is, displays a darker-than-50% gray-scale light-transmission level below the black bar, and a brighter-than-50% gray-scale light-transmission level above the black bar. This is in 180° phase contrast compared to the color pixel for the case of $\alpha > \beta$. Above the color (black) bar, the color (black)-bar data-line pixels are lighter (darker), and below the color (black)-bar data-line

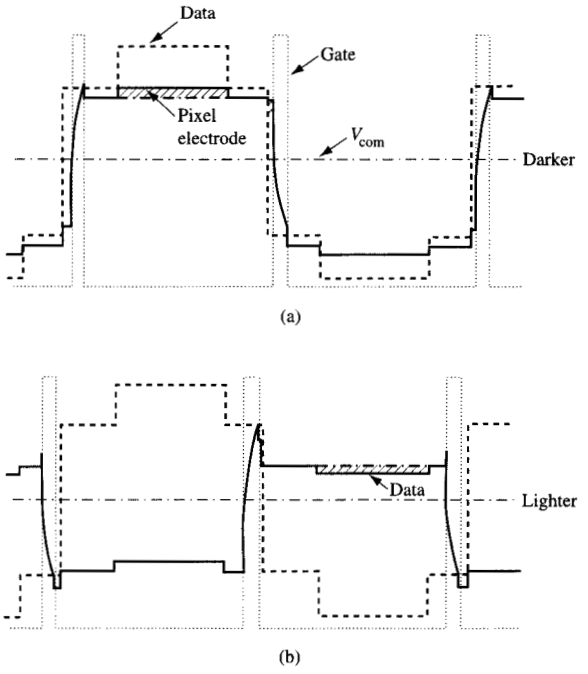

Figure 14

DI driving method pixel waveform voltages, with $\alpha > \beta$, for two regions corresponding to the black-bar data-line pixels (a) above and (b) below the black-bar pattern of Figure 1.

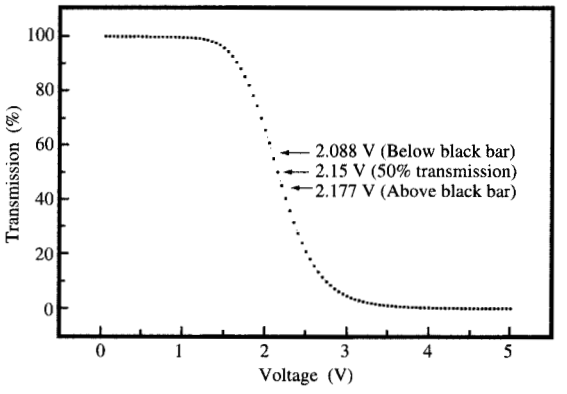

Figure 15

Transmission vs. voltage data with crosstalk simulation voltages, with $\alpha = 0.08$ and $\beta = 0.03$, for the region corresponding to the black-bar data-line pixels below and above the black-bar pattern of Figure 1.

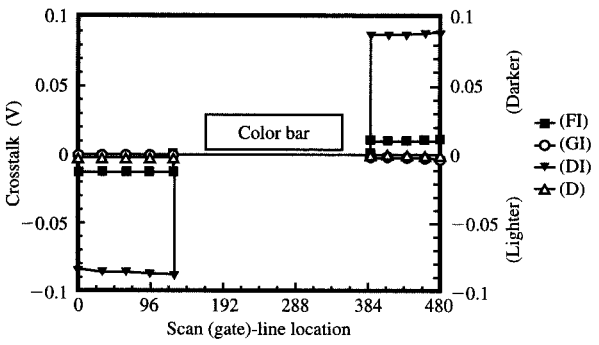

Figure 16

Simulations with $\alpha = 0.08$ and $\beta = 0.03$, showing crosstalk vs. gate-line locations for the FI, GI, DI, and D driving methods, for a color-bar pattern image spanning gate lines 126 through 384 in a VGA display.

pixels, the pixels are darker. Figure 15 shows the results of simulations for $\alpha = 0.08$ and $\beta = 0.03$. Therefore, for a DI-driven display, only the black-bar test pattern carries information about the relative magnitudes of α and β.

As stated earlier, $\alpha \approx \beta \approx 0.04$, as calculated from the layout. As seen from Equation (5), if $\alpha = \beta$, no first-order crosstalk is expected if the DI driving method is used. The display of Figure 1 shows substantial crosstalk, indicative of $\alpha \neq \beta$. The most probable explanation for the crosstalk in that display is either 1) a misalignment of the pixel electrode to the right or to the left with respect to the data line, resulting in $\alpha < \beta$ or $\alpha > \beta$, respectively; or 2) cell capacitance discharge via TFT-photogenerated leakage from backlight illumination, resulting in $\alpha > \beta$. Since the parasitic capacitive coupling is relatively small compared to other capacitances such as C_S, a small change in the fabrication process can produce large changes in α and β. Factors such as over-etching of the pixel electrode can increase S and decrease both β and, to a lesser extent, α, since over-etching the pixel ITO layer does not change the TFT data metal source-to-drain coupling component incorporated in α. Over-etching of the data metal should have a negligible effect, since the underlying n^+ a-Si:H conductive layer geometry has a high etching selectivity during the data metal etching and should therefore remain intact. For example, a 0.5-μm-pixel ITO electrode over-etching accompanied by a 1-μm misalignment to the left yields $\alpha \approx 0.045$ and $\beta \approx 0.032$.

Figure 16 shows the simulated crosstalk vs. gate-line location for a color-bar pattern image spanning gate lines 126–384 in a VGA display. Simulation parameters of $\alpha = 0.08$ and $\beta = 0.03$ have been used for the noted FI, GI, DI, and D driving methods. Note that the crosstalk shown is the absolute difference from a 50% transmission reference pixel selected by the same gate line to an intended 50% transmission operating point for pixels on a color-bar-producing data line that runs vertically through the color bar. The gradual lateral top–bottom background gray-scale variation mentioned earlier is excluded for clarity. As suggested by the simulations, the GI and D driving methods should produce approximately zero crosstalk. Compared to the GI driving method, the D driving method requires either higher-voltage data drivers or double-sided data-driver tabbing to the panel. The near-zero crosstalk simulations have been experimentally confirmed for the D driving method.

Conclusions

The following can be concluded from this work:

1. Scaling toward higher-density (more dpi) and/or higher-gray-scale displays will significantly increase the parasitic data-line-to-pixel-electrode coupling. This capacitive coupling increase is directly proportional to a vertical crosstalk increase.
2. Experimental determination of the relative magnitude of the parasitic capacitive coupling ratio responsible for crosstalk through a front-of-screen image is possible. For example, a front-of-screen image can be a red, green, blue, and black bar on a gray background, with attention paid to the regions above and below these bars. A second pattern is required to determine the coupling ratios when GI and D inversion drive schemes are used. Since all four driving methods (DI, FI, GI, D) depend on the front-of-screen pattern, the second pattern should be identical to the first, except where the color bars for that pattern would be composed of horizontal alternating color on, followed in the next scan line of color off.
3. Quantitative analysis of crosstalk can be described accurately for the commonly used front-of-screen color and monochrome bar patterns using the mathematical formulations presented here.
4. For the display of Figure 1, based on the front-of-screen pattern produced with the DI driving method, $\alpha > \beta$. For a DI-driven display, the black-bar test pattern carries information about the relative magnitudes of α and β, but the color-bar test pattern does not. Similar information on the magnitudes of α and β can be obtained using the other driving methods.

Acknowledgments

We wish to acknowledge the members of the Flat Panel Processing group and the Flat Panel Drive Electronics group for their contributions in the fabrication, cell-fill

process, and module electronics that provided the 5.5-in.-diagonal displays characterized in this study. In addition, thanks are extended to R. Nywening for help with photography.

References

1. F. R. Libsch and S. A. Lien, *Digest of Technical Papers*, Society for Information Display International Symposium, 1995, p. 17.1.
2. F. R. Libsch and A. Lien, *Jpn. J. Appl. Phys.* **34,** 6364 (1995).
3. S. Takahashi, S. Shibata, K. Gondo, S. Yachi, Y. Ohno, T. Tobita, and H. Takasago, *Digest of Technical Papers*, Society for Information Display International Symposium, 1994, p. 463.
4. Y. Kato and Y. Hayashi, *Digest of Technical Papers*, Society for Information Display International Symposium, 1996, p. 554.
5. P. Fryer et al., *Proceedings of the 1994 International Display Research Conference* (Society for Information Display), 1994, p. 146.
6. L. Palmateer, *Digest of Technical Papers*, Society for Information Display International Symposium, 1994, p. 441.
7. K. C. Gupta, R. Gag, and I. J. Bahl, *Microstrip and Slotlines*, Artech, New York, 1979, and references therein.
8. W. E. Howard and P. M. Alt, U.S. Patent 4,845,482, July 4, 1989.
9. W. E. Howard, P. M. Alt, and R. L. Wisnieff, *Proceedings of the 1988 International Display Research Conference* (Society for Information Display), 1988, p. 230.

Received April 25, 1997; accepted for publication February 6, 1998

Frank R. Libsch *IBM Research Division, Thomas J. Watson Research Center, P.O. Box 218, Yorktown Heights, New York 10598 (libsch@us.ibm.com).* Dr. Libsch received a B.S. degree in 1982, an M.S. degree in 1984, and a Ph.D. degree in 1989 from Lehigh University, all in electrical engineering. In 1989, he joined IBM at the Thomas J. Watson Research Center, where, as a Research Staff Member, he has worked on aspects of drive schemes and electronics, pixel designs, CMOS FETs and TFTs, and their application in various direct-view and projection, transmissive and reflective flat-panel displays. Dr. Libsch currently manages a group engaged in advanced flat-panel display devices, processes, and testing research. He holds several U.S. and foreign patents and is the author or coauthor of more than 50 technical publications, including a recent book chapter entitled "SONOS Nonvolatile Semiconductor Memories" in the book *Nonvolatile Semiconductor Memory Technology*. Dr. Libsch is a member of the IEEE, the Society for Information Display, the New York Academy of Sciences, and Sigma Xi. He currently serves as the chairperson of the AMLCD Subcommittee of the Society for Information Display and as a member of the Executive Committee of the Society for Information Display.

Shui-Chih Alan Lien *IBM Research Division, Thomas J. Watson Research Center, P.O. Box 218, Yorktown Heights, New York 10598 (salien@us.ibm.com).* Dr. Lien received a B.S. degree in physics from the National Taiwan Normal University, Taipei, Taiwan, in 1977, and an M.S. degree in electrical engineering and a Ph.D. degree in physics from the University of Minnesota, Minneapolis, in 1984. From 1984 to 1987, he worked at Optical Imaging Systems, Inc., Troy, Michigan, where he was involved in the development of large-area active-matrix liquid crystal displays. In 1987, Dr. Lien joined IBM at the Thomas J. Watson Research Center, where he is currently a Research Staff Member in the Flat Panel Display Technologies group. His research interest is in liquid crystal display physics and technology. He is an author or coauthor of five U.S. patents and 70 technical papers. Dr. Lien is currently a member of the Board of Directors of the International Liquid Crystal Society and a member of the Liquid Crystal Technology Subcommittee of the Society for Information Display.

[[Page 480 is blank]]